IRANIAN JOURNAL OF CATALYSIS

Applying Taguchi method to optimize the synthesis conditions of $ZrO_2/TiO_2/ZnO$ nanocomposite for high-performance photodegradation of Congo red

Toktam Seyedi-Chokanlou,[a] Shokufeh Aghabeygi,[a]* Nasibeh Molahasani,[a] Fahimeh Abrinaei[b]

a) Department of Chemistry, East Tehran Branch, Islamic Azad University, Tehran, Iran
b) Department of Physics, East Tehran Branch, Islamic Azad University, Tehran, Iran

Received 2 June 2020; received in revised form 13 January 2021; accepted 14 January 2021

ABSTRACT

In this work, $ZrO_2/TiO_2/ZnO$ ternary nanocomposites were prepared by the sol-gel technique. The Taguchi method with the L_9 orthogonal array was utilized to optimize the experimental conditions for the preparation of nanocomposites. The $L_9(3^4)$ design has four factors, and each factor has three levels. The design factors of this study were calcination temperature, the aging time, the calcination time, and ultrasonic irradiation duration. Furthermore, as-synthesized structural features of nanocomposites were characterized, utilizing XRD, BET, FESEM, and EDX. The photocatalytic activities of all $ZrO_2/TiO_2/ZnO$ nanocomposites were evaluated by the photodegradation of Congo red (CR) as an azo dye. The photocatalytic property of nanocomposites was enhanced by decreasing particle size and increasing the surface area. The best sample photodegraded 97% the CR solution within 15 min under an 8W UV lamp. The optimal conditions were achieved as 400 ºC calcination temperature, 72 h aging time, 4 h calcination time, and 30 min duration of ultrasonic irradiation for CR solution photodegradation. The effect of each parameter was evaluated using ANOVA analysis. The kinetics results showed the pseudo-first-order reaction mechanism for the photocatalytic activities of the nanocomposites.

***Keywords**: Taguchi method; Synthesis condition; Optimization; Photodegradation; $ZrO_2/TiO_2/ZnO$ nanocomposite.*

1. Introduction

Organic synthetic dyes are the most polluted in the wastewater textile industry. Therefore, the purpose of some environmental researchers is to depredate and mineralize azo dyes. The dyes in wastewater should be treated first before release to minimize their negative impacts on the environment and living things [1-3]. Different methods such as biological oxidation [4], membrane separation [5, 6], electrochemical [7], bioelectrochemical [8], ozonation [9], sonocatalytic degradation [10], and photodegradation [11] have been used for removing the pollutants from water and wastewater samples. Congo red (CR) dye is an anionic azo dye with a wide range of uses in the textile industry and laboratory applications. It is a water-soluble and potentially toxic compound. Thus, CR can be dangerous to humans and all life-body safety. Thus, it must be removed from the wastewater and ecosystems [12, 13]. For decades, ZnO, TiO_2, ZrO_2, and their binary composites have been widely utilized as photocatalysts, but their ternary compounds have been less investigated. These photocatalysts have frequently been used for the photodegradation of wastewater. The advanced oxidation process (AOP) based on photocatalysts has recently been applied to degrade organic pollutants. The main advantage of using the AOP technique is that it transforms the toxic organic pollutants into nontoxic products like CO_2 and H_2O. Heterogeneous photocatalysts is a branch of AOP where a semiconductor catalyst under UV irradiation is highly successful in mineralizing aromatic compounds [3, 14-16]. The photocatalytic mechanism is based on the generation of electron/hole (e-/h+) pair. Then the h^+/e^- is caused to produce the hydroxyl radical. Hydroxyl radicals attack organic molecules through three possible means: (i) dehydrogenation of a hydrogen atom to form H_2O, (ii) hydroxylation of an unsaturated bond, and (iii) redox reaction [2]. The composition of semiconductor photocatalysts increases the separation of h^+/e^- consequently resulting in higher photocatalytic activity [17, 18]. The main advantage of heterogeneous catalysts

*Corresponding author:
E-mail address: *saghabeygi@yahoo.com* (Sh. Aghabeygi)

is that they are easily separated from the solution and can be reused repeatedly. However, the disadvantage of heterogeneous catalysts is that only the surface of the catalyst is used [3].

The Taguchi method can employ the optimization of the design parameters by an orthogonal array (OA). It is a statistical approach for designing experimental conditions, which provides a mathematically independent assessment of the different factors' effects on the response factor. This systematic approach can considerably reduce the overall time and the expenditure of experiments. In the Taguchi method, the results of the experiments are analyzed to obtain the conditions for synthesizing the best product. Analysis of variance (ANOVA) is used to clear up the experiments' results and determine the most significant factors on photocatalytic activity [19-21].

Herein, we report the sonosynthesis of the $ZrO_2/TiO_2/ZnO$ (ZTZ) nanocomposites, which have not been sonosynthesized and used as photocatalyst for photodegradation of Congo red (CR). The aims of this research were (1) to apply the Taguchi method for designing the conditions of sonosynthesis of ZTZ nanocomposites for approaching higher photodegradation of Congo red and (2) to evaluate the effect of particle size on the photodegradation properties.

2. Experimental

2.1. Materials

Zirconium (IV) chloride anhydrous (99.0%), ammonium solution (28 %), 2-propanol (99.5 %), acetic acid (99%), ethanol (95 %), titaniumtetraisopropoxide (97 %) and zinc acetate dihydrate (98 %) were purchased from Merck Company.

2.2. Characterization methods

The ZTZ nanocomposites were characterized by a Field Emission Scanning Electron Microscopy (FESEM) coupled with energy-dispersive X-ray spectroscopy (EDX) (Hitachi S4160, Cold Field Emission) with preliminary gold coating. X-ray powder diffraction (XRD) of ZTZ samples performed using an X'pert diffractometer with monochromatized CuKα radiation ((Philips Company). UV-Vis spectrometer (Varian, Carry 100 Bio) was used for photodegradation analysis. The Brunauer–Emmett–Teller (BET) measurements were done by nitrogen adsorption in a NOVA 4000e (Quanta-chrome Instruments).

2.3. Experimental design

In this work, four controllable factors, including calcination temperature, aging time, calcination time, and ultrasonic irradiation duration with each factor in three levels (**Table 1**), were used as the design factors for the synthesis of ZTZ ternary nanocomposites. The ZTZ nanocomposites were employed for photodegradation (PD) of CR.

Table1. The controllable factors and their levels

Factors	Description	Levels		
		1	2	3
A	Calcination temperature(ºC)	300	400	600
B	Aging time (h)	24	48	72
C	Calcination time (h)	2	4	6
D	Duration of ultrasonic irradiation (min)	5	15	30

An L_9 orthogonal array (OA) was employed, and the experimental conditions (**Table 2**) were obtained by matching **Table 1** and the L_9 (3^4) OA. Four factors, each in three levels, were used to synthesize nine nanocomposites and photodegradation (PD).

Table2. Experimental conditions based on the Taguchi method

No.of sample	Factor A (level)	Factor B (level)	Factor C (level)	Factor D (level)	%PD
1	300(1)	24(1)	2(1)	5(1)	78
2	300(1)	48(2)	4(2)	15(2)	84
3	300(1)	72(3)	6(3)	30(3)	92
4	400(2)	24(1)	4(2)	30(3)	97
5	400(2)	48(2)	6(3)	5(1)	90
6	400(2)	72(3)	2(1)	15(2)	91
7	600(3)	24(1)	6(3)	15(2)	79
8	600(3)	48(2)	2(1)	30(3)	82
9	600(3)	72(3)	4(2)	5(1)	76

2.4. Sonosynthesis of $ZrO_2/TiO_2/ZnO$ nanocomposites

The sol-gel method was used to synthesize the ZTZ nanocomposites. The sol mixtures of zinc, zirconium, and titanium were blended in the same ratio, and then the ZTZ nanocomposites were prepared based on the described experimental conditions in **Table 2**.

Preparation of ZrO_2 sol: Firstly, 0.01mol (2.3 g) $ZrCl_4$ was dissolved in 50 mL distilled water. Then the pH of the solution reached 9 by dropwise addition of NH_4OH solution under stirring. The zirconium sol was formed as a white suspension as described in **Eq. (1)** and **(2)** [22]:

$$ZrCl_4 + 4\,NH_4OH \rightarrow Zr(OH)_4 + 4\,NH_4Cl \quad \textbf{(1)}$$

$$Zr(OH)_4 + 2\,NH_4OH \rightarrow Zr(OH)_6^{2-} + 2\,NH_4^+ \quad \textbf{(2)}$$

Preparation of TiO_2 sol**:** First, 0.01 mol (3 mL) titaniumtetraisopropoxide (TTIP) was dissolved in 20 mL 2-propanol (solution A). The distilled water, acetic

acid, and ethanol were added together in the same ratio (solution B). After that, the solution B was dropped into solution A under stirring. The mixture was stirred for 1h to obtain a pale yellow transparent titanium sol as presented in **Eq. (3)** [23]:

$$Ti(O-iPr)_4 + 4\,H_2O \rightarrow Ti(OH)_4 + 4\,i-prOH \quad \textbf{(3)}$$

Preparation of ZnO sol: Firstly, 0.01 mol (2.2 g) $Zn(CH_3COO)_2.2H_2O$ was dissolved in 50 mL distilled water. Then NH_3 (aq) solution (1M) added drop wise under stirring into the zinc acetate solution until the white precipitate of $Zn(OH)_2$ appeared, and pH was adjusted 9. Further addition of ammonium solution dissolved the precipitate. Consequently, the white zinc sol formed as below (**Eq. (4)**):

$$Zn(CH_3COO)_2 + 4\,NH_4OH \rightarrow Zn(OH)_4^{2-} + 4\,NH_4^{+} + 2\,CH_3COO^{-} \quad \textbf{(4)}$$

Finally, the prepared sols of zinc, titanium, and zirconium were directly mixed, and the designed factors (based on **Table 2**) were employed to achieve the nine ZTZ nanocomposites. An ultrasound horn (Bandelin, SONOPULS, 20 kHz) was used at 100% amplitude and delivering the power of 200W for sonication of solution [24].

2.5. Photocatalytic process

For the evaluation of photocatalytic activities of the as-synthesized ZTZ nanocomposites, the CR solution was employed as a water pollutant model. The photodegradation reaction was conducted at room temperature under the UV8W tube. The photocatalytic degradation was calculated by decreasing the absorption intensity of CR solution at wavelength $\lambda_{max} = 502\ nm$ with an initial concentration of 10 ppm (**Fig. 1**). In each experiment, 0.05g of photocatalyst dispersed into the 100 mL CR solution. The following equation calculated the percent of dye photocatalytic degradation (% PD) (**Eq. (5)**):

$$\%\,PD = \frac{Ao - A_t}{Ao} \times 100 \quad \textbf{(5)}$$

where A0 is the initial absorbance of CR solution, and A_t is the absorbance of the CR solution after irradiation time (t). Adsorption capacity Xm (mg/g) calculated using the following formula (**Eq. (6)**) [25]:

$$X_m = \frac{(C_0 - C_t)\times V}{W} \quad \textbf{(6)}$$

where C_0, C_t, V, and W are the initial concentration of CR solution, the CR solution concentration after irradiation time t, the volume of CR solution, and the mass of photocatalyst, respectively.

3. Results and Discussion

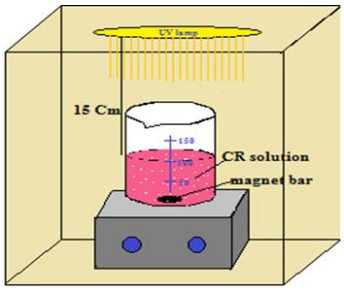

Fig.1. Instrumental set up for photodegradation of CR solution**.**

3.1. FESEM images and EDX analysis

The surface morphology and particle size of synthesized ZTZ nanocomposites were investigated via FESEM imaging. As seen in **Fig. 2**, the nanocomposites have a spherical shape with a smooth surface. As it is well known, the particle size is significant on both surface area and the photocatalytic properties. If the particle size decreases, the specific surface area and the adsorption of dye molecules on the surface of the catalyst enhance, and then the photocatalytic activity increases. The average particle size was increased with the enhancement of calcination temperature because the particles were agglomerated by increasing the calcination temperature. With the increase in the ultrasonic irradiation time, the particle size and the value of byproducts reduced [26-28]. As shown in histogram diagrams of **Fig. 2**, the particle size of ZTZ nanocomposites was enhanced by decreasing the ultrasonic irradiation time and increasing the calcination temperature.

Table 3 gives the elemental analysis of ZTZ nanocomposites using Electron Dispersive X-ray Spectroscopy (EDX). The EDX data shows that the ratios of elements are similar to each other in all samples. The material ratios have been equal, and there were no differences between the compositions of ZTZs nanocomposite. On the other hand, the different proportions of nanomaterials in nanocomposite can be a significant function in the photocatalytic properties of nanocatalysts. The Eg of ZnO and TiO_2 is smaller than ZrO_2. Therefore, increasing ZnO and TiO_2 can be caused by decreasing the Eg catalyst and raising photocatalytic activities of catalysts.

3.2. XRD results

Fig. 3 represents the XRD patterns of ZTZ nanocomposites 1 to 9. All samples exhibited the typical pattern for the tetragonal structure of ZrO_2 (ref. code 01-088-1007with P42/nmc space group, JCPDS # 17-923), with characteristic planes of (101), (110),(112), (200), and (211) at 2θ: 30.10°,35.39°, 50.33°, 50.73°, and 60.22°, respectively. Also, the peak at 25.19°, 37.55°,

47.39°, 53.56°, and 54.87° indicated the crystal planes of (101), (004), (200), (105), and (211) anatase crystalline structure of TiO_2 (ref. code 01-071-1167, with I41/amd space group, JCPDS # 21-1272). The ZTZ nanocomposites show hexagonal wurtzite structure of ZnO (ref. code 01-080-0074, with P63mc space group, JCPDS # 36-1451) with characteristic planes of (100), (002), (101), (110) and (103) at 2θ: 31.63°,34.37°, 36.20°, 56.41°, and 62.65°. A slight difference was observed in peak intensities and position due to the difference in the preparation condition of nanocomposites. The average crystallite size of ZTZ nanocomposites (Dv) was calculated based on the XRD pattern using the Debye- Scherer equation (**Eq. (7)**) [29]:

$$Dv = \frac{K\lambda}{\beta \cos\theta} \quad (7)$$

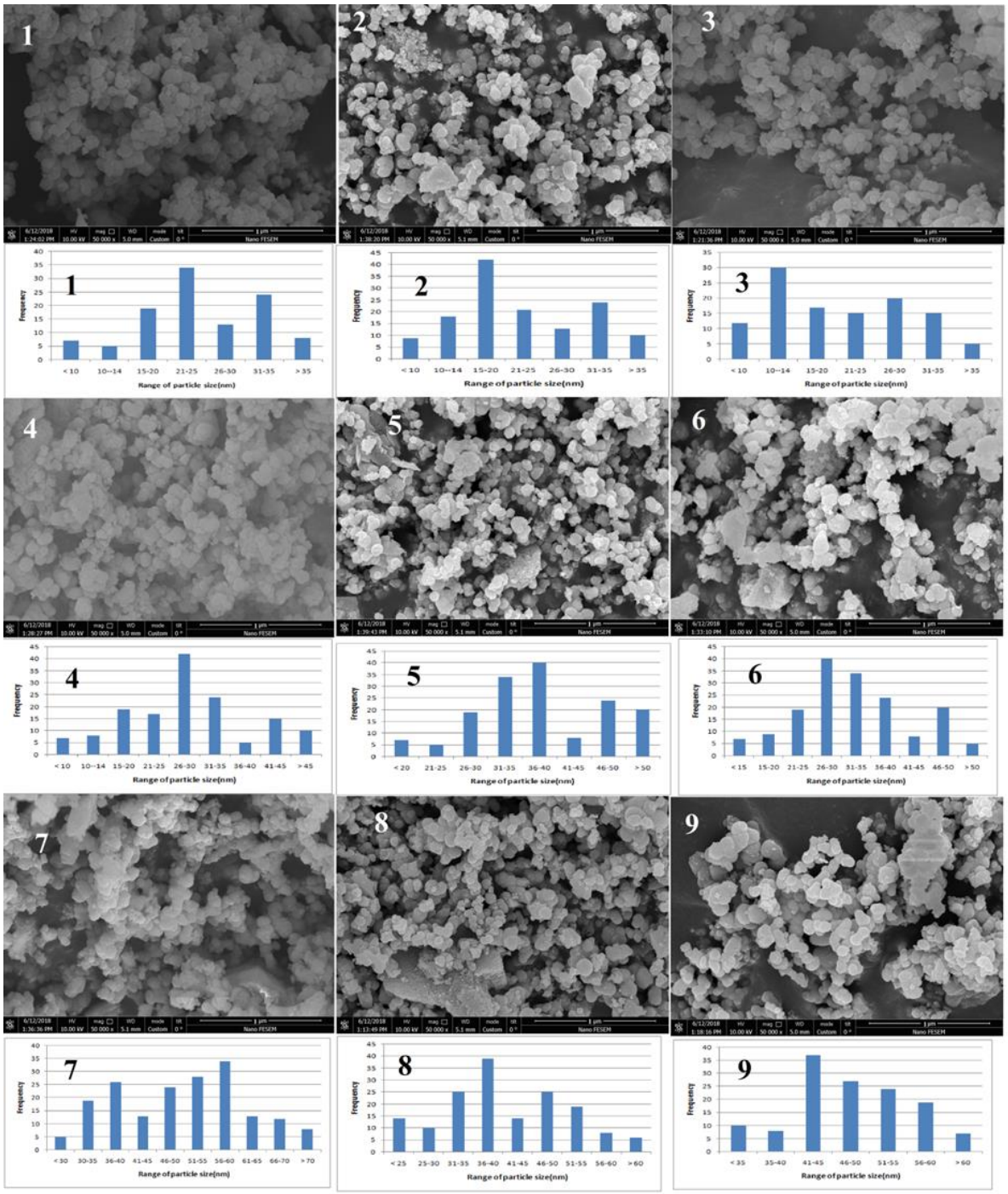

Fig.2. FESEM images and particles size histograms of ZTZ nanocomposites

Table 3. EDX data of the as-synthesized ZTZ nanocomposites

Element	Zn		Ti		Zr		O	
Sample	norm C [wt%]	Atom C[at%]	norm C [wt%]	Atom C[at%]	norm C [wt%]	Atom C[at%]	norm C [wt%]	Atom C[at%]
ZTZ1	22.21	11.50	17.35	14.26	32.19	13.33	27.82	60.91
ZTZ2	23.14	11.98	15.56	12.79	35.14	15.11	26.16	59.32
ZTZ3	23.17	11.99	16.83	13.83	33.05	14.49	26.95	59.20
ZTZ4	22.71	11.80	17.54	15.13	32.88	13.89	26.87	59.18
ZTZ5	21.95	11.41	16.77	13.35	34.56	15.12	26.72	60.12
ZTZ6	21.78	11.32	17.90	14.67	33.26	14.39	27.06	59.62
ZTZ7	22.63	11.76	16.84	13.51	35.75	15.22	24.78	59.51
ZTZ8	23.01	11.96	15.42	12.97	32.95	13.89	28.62	61.18
ZTZ9	21.82	11.35	17.68	14.43	34.13	14.61	26.37	59.61

where Dv is the crystallite size, K is the Scherer constant, λ is the CuK_{α}= 1.541 Å, β is the FWHM, and θ is the Bragg angle. The value of the dislocation density (δ) of the matter is a measure of the crystal number of defects [27, 30]. The dislocation density is calculated using the following equation (**Eq. (8)**):

$$\delta = \frac{1}{D_v{}^2} \qquad \textbf{(8)}$$

The crystallite size and dislocation density of samples are given in **Table 4**. As shown in **Fig. 3**, at low temperature, all the peaks are broad that representing the crystallite size is small. While the calcination temperature increases from 300 ºC to 600 ºC, the peaks became sharper, indicating the larger crystallite size [31].

3.3. Williamson-Hall (W-H) model

One of the simplest models for analyzing the relation between crystallite size and strain is the Williamson-Hall model. The strain influences the crystallite size by inducting line broadening. The equation (9) is known as the W-H equation, called the Uniform Deformation Model (UDM). In this model, the crystal is considered isotropic, which undergoes uniform strain in all crystallographic directions (**Eq. (9)**).

$$\beta_{hkl}cos\theta_{hkl} = \frac{k\lambda}{D_v} + 4\varepsilon sin\theta_{hkl} \qquad (\textbf{9})$$

where $\beta_{hkl}$is the half-maximum intensity of instrumental corrected broadening. The UDM plot of ZTZ4 is shown in **Fig. 4**. The consideration of the homogeneity and isotropic nature is not valid in all cases. Hence, the W-H equation is modified with the anisotropic strain and is known as the Uniform Stress Deformation Model (USDM). In this model, stress is assumed to be uniform in all crystallographic directions. This assumption is valid only for small strain. The crystallite size of ZTZ4 (29.13 nm) was calculated by using the intercept of the curve (**Fig. 4**). The crystallite size values are similar in using the Debye- Scherer equation and W-H method [30].

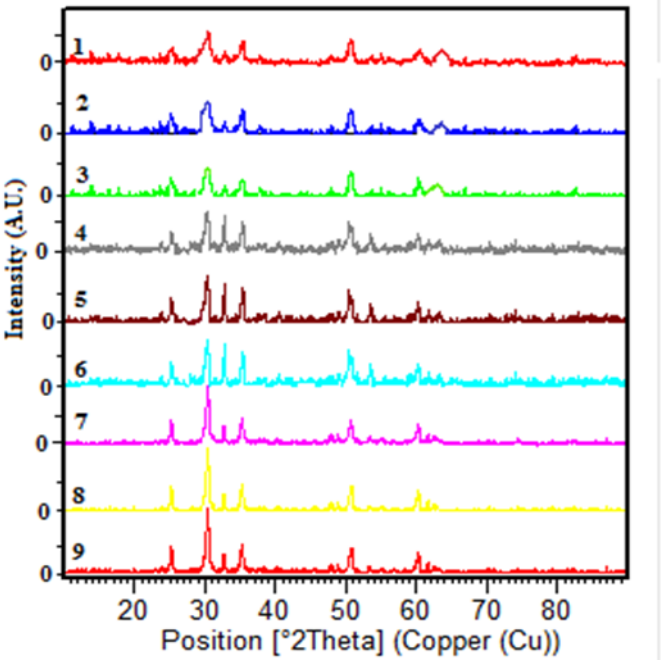

Fig. 3. XRD pattern of the as-synthesized ZTZ nanocomposites

Table 4. Crystallite size, dislocation density, BET, and C_F of ZTZ nanocomposites

sample	Average crystallite size (nm)	Dislocation density x10^{14} (line/m^2)	BET Surface area (m^2/g)	C_F agglomeration coefficient
ZTZ1	15.4	42.17	44.6	1.57
ZTZ2	13.1	58.27	52.1	1.56
ZTZ3	12.3	66.09	55.1	1.55
ZTZ4	18.6	28.90	36.4	1.58
ZTZ5	24.2	17.08	27.7	1.60
ZTZ6	21.5	21.63	31.3	1.59
ZTZ7	31.9	9.83	20.9	1.63
ZTZ8	26.2	14.57	25.6	1.62
ZTZ9	27.6	13.13	23.8	1.61

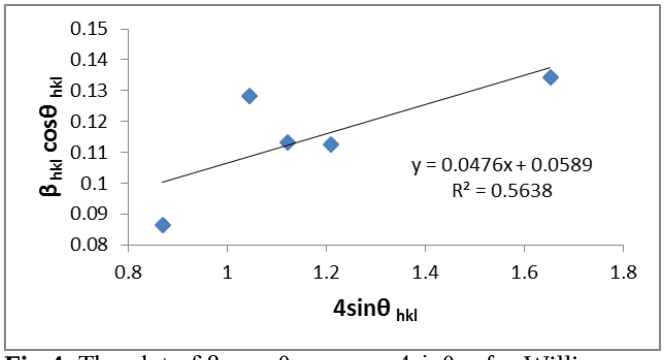

Fig 4. The plot of $\beta_{hkl}\cos\theta_{hkl}$ versus $4\sin\theta_{hkl}$ for Williamson-Hall (W-H) analysis of the best sample ZTZ4

3.4. BET measurements

The specific surface area of the ZTZ nanocomposites was obtained from the BET procedure. The results of the specific surface area are given in Table 3. The specific surface area (S_{BET}) gives the average particle diameter by **Eq. (10)**:

$$d_{BET} = \frac{6000}{\rho\, S_{BET}} \qquad \textbf{(10)}$$

where d_{BET} is the particle size, ρ is the density in g/cm^3, and S_{BET} is the specific surface area in m^2/g. The fine particles tend to become agglomerates together in the synthesis process. The S_{BET} depends on the attractive force between the particles and nitrogen molecules that could access a larger or smaller area. Thus, this method gives the approximate values for the particle size. The agglomeration coefficient (C_F) can be calculated using the following formula (**Eq. (11)**):

$$C_F = \frac{d_{BET}}{D_v} \qquad \textbf{(11)}$$

where C_F, d_{BET}, and Dv are the agglomeration coefficient, the average crystallite size determined by the BET methods, and the XRD Debye-Scherer formula [32, 33].

3.5. Statistical Analysis

Usually, the signal to noise (S/N) ratio was utilized to evaluate the experimental data with three types: (1) the smaller is better (SB), (2) the medial is better (MB), and (3) the larger is better (LB). Since the aim of this research is to maximize photodegradation; the S/N ratio with LB criteria is utilized as below (**Eqs. (12), (13)**):

$$\frac{S}{N} = -10\log\left(\frac{1}{n}\sum_{i=1}^{n}\frac{1}{Y_i^2}\right) \qquad \textbf{(12)}$$

$$(M)_{factor=I}^{level=i} = \frac{1}{n_{Ii}}\left[\sum_{j=1}^{n_g}\left(\frac{S}{N}\right)_{factor=I}^{level=i}\right]_j \qquad \textbf{(13)}$$

After the experimental evaluation of photodegradation, the design expert software was used to calculate the S/N ratio of the main effect graphs for various designed experiments, as shown in **Fig. 5** [19-21].

It is noticeable that calcination temperature and duration of ultrasonic irradiation have more effects than the aging time and calcination time on the photocatalytic activity of catalysts.

The values of "Prob > F" less than 0.0500 for a model term indicate its significance in the model. In this research, factor A(calcination temperature) and factor D (duration of ultrasonic irradiation) are the most important models. Factor C (calcination time) has the least effect, and factor B (aging time) has little effect on the photodegradation process. **Table 5** shows the experiment results evaluated by analysis of variance

(ANOVA). The ANOVA determines the effect of each parameter on the variance of the response. The results show that the most important factor contributing to the CR degradation is the temperature of calcination, followed by the duration of ultrasonic irradiation, the aging time, and lastly, calcination time [21].

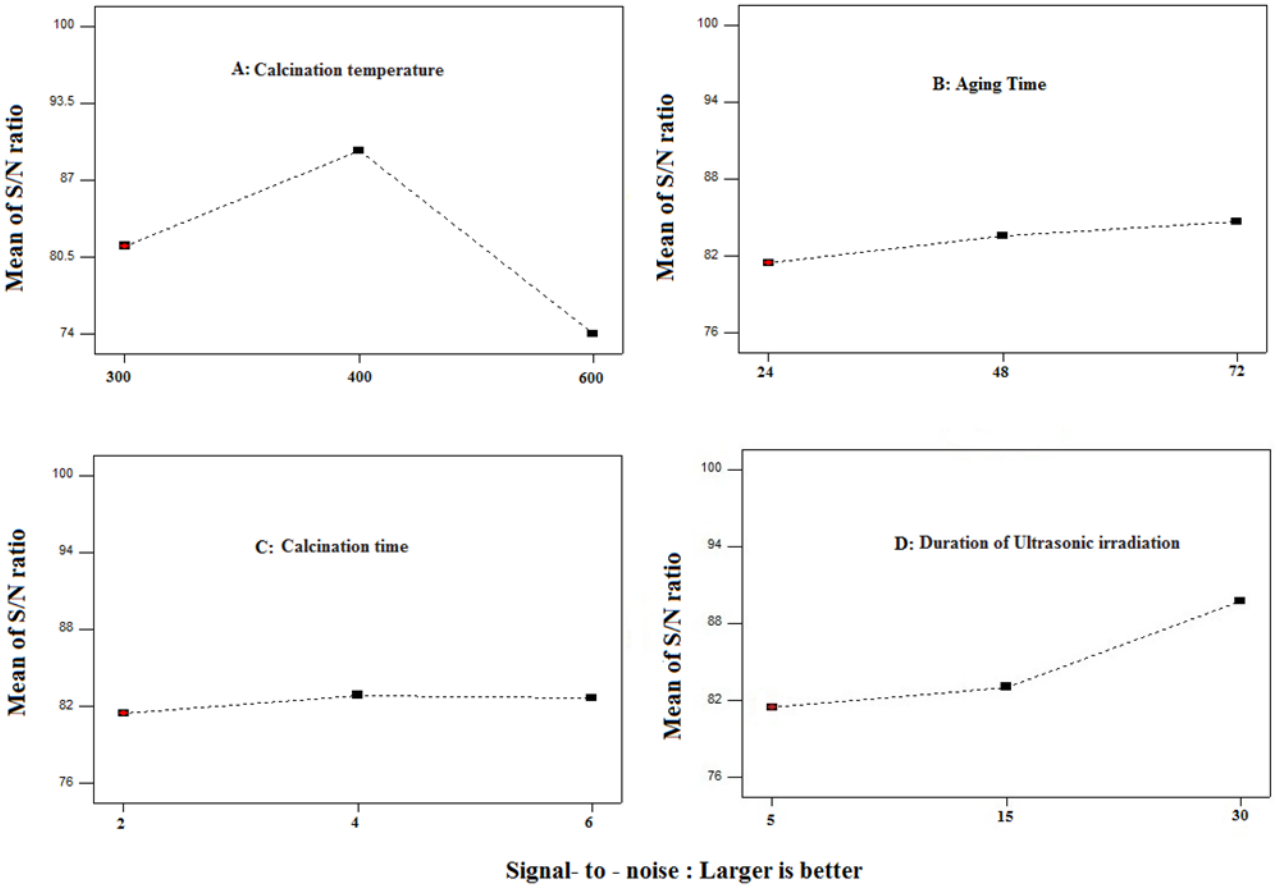

Fig. 5. Effects of four factors on the signal to noise of the photodegradation process

Table 5. ANOVA results for experimental responses in the photocatalytic process

Factor	Sum of squares	Degree of freedom	Mean square	F-value	P-value(Prob>F)
A	359.94	2	179.97	102.01	0.0097
B	15.96	2	7.98	4.52	0.1810
C	3.53	2	1.75	0.22	0.8190
D	115.54	2	57.77	32.74	0.0296
Total	494.97	8			

The calcination temperature, the aging time, calcination time, and duration of ultrasonic irradiation have affected nanocomposites' photocatalytic activity differently.

3.6. Effect of calcination temperature

As seen in **Fig. 5**, the best S/N ratio was for a calcination temperature of 400 ºC. There is a general agreement in the literature, which confirms that the optimal calcination temperature is near 400 ºC. By increasing calcination temperature from 400ºC to 600ºC, the S/N ratio has considerably reduced. It can be explained by the effect of the calcination temperature on the particle size. Generally, the size of particles increases with increasing the calcination temperature because the particles were aggregated. Moreover, the specific surface area of photocatalyst decreases as the particle size increases [34].

3.7. Effect of the duration of ultrasonic irradiation

As shown in **Fig. 5**, the S/N ratio was increased as enhancing the duration of ultrasonic irradiation from 5 min to 30 min. The purity of nanoparticles increased with enhancing the sonication time. Furthermore, the size of the particles was decreased by increasing ultrasonic irradiation time [26-28].

3.8. Effect of aging time

The reaction time is an influential factor in the completion of the reaction, so the S/N ratio raised as increasing the aging time from 24 h to 72 h (**Fig. 5**). The average grain size of ZTZ nanocomposites increased with the increment of aging time. It is due to the small crystallites blending to produce large crystallites. These results indicate that while the sol aging time increases, the particles joined due to enhancement in the viscosity of the sol [35].

3.9. Effect of calcination time

Fig. 5 shows that the S/N ratio increases with the enhancing of calcination time up to 4h, and then it decreases by increasing the time. In short during calcination times, the volatile compounds remain in the nanocomposites and act as photocatalyst poisons. On the other hand, the longtime of calcination aggregate the particles, and then the efficiency of catalysts reduces by reducing the active surface area [28].

3.10. Photodegradation results

Fig. 6 shows the photodegradation efficiency of ZTZ nanocomposites on photodegradation of CR solution under UV irradiation. The greatest photodegradation of CR solution was obtained by the ZTZ 4 nanocomposite so that the dye photodegradation reached 97% within 15 min. In the blank test, the CR solution was rarely photodegraded with less than 2% decomposing efficiency during 15 min of UV irradiation.

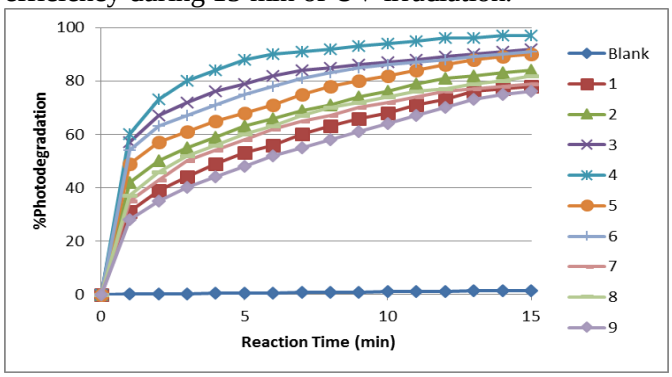

Fig. 6. The plot of photodegradation of CR solution versus reaction time for the as-synthesized ZTZ nanocomposites

3.11. Kinetic study of photodegradation

It has reported the photocatalytic mineralization of most azo dyes follows Langmuir-Hinshelwood kinetic model [31, 32, 36] commonly stated as (**Eq. (14)**):

$$-\frac{dC}{dt} = \frac{kKC}{1+KC} \qquad \textbf{(14)}$$

where C is the concentration of reactant, t represents the reaction time, k denoting the rate constant of the reaction (min^{-1}), and K is the absorption coefficient of the reactant. When C is very small, the equation (**14**) can simplify to pseudo-first-order kinetics as below (**Eqs. (15), (16)**)

$$-\frac{dC}{dt} = kKC = k_{ap}\, C \qquad \textbf{(15)}$$

$$-ln\frac{C_t}{C_0} = k_{ap}\, t \qquad \textbf{(16)}$$

where C_t and C_0 represent the concentration of CR solution at time t and 0, k_{ap} is the rate constant of pseudo-first-order reaction (min^{-1}), and t shows the reaction time. In this research, all of the data has confirmed that the reaction is pseudo-first-order (**Table 6**). As mentioned above, the photodegradation of CR solution accords with pseudo-first-order kinetics. As shown in **Fig. 7**, the slope of the plot of $-ln\frac{C_t}{C_0}$ versus reaction time (t) has yielded the rate constant. The rate constant (k), standard deviation (R^2), half time ($t_{1/2}$) of photodegradation process, and adsorption capacity (X_m) of photocatalysts are summarized in **Table 6**. The ZZ4 nanocomposite has the highest rate constant, the lowest half time, and the largest adsorption capacity, which agrees with characterization results. Furthermore, the adsorption capacity of a catalyst depends on the specific surface area and the photodegradation rate. The increasing of the adsorption capacity of the photocatalyst enhanced the photodegradation efficiency because the adsorption of the azo dye molecules on photocatalyst is necessary for the photodegradation process (**Table 6**).

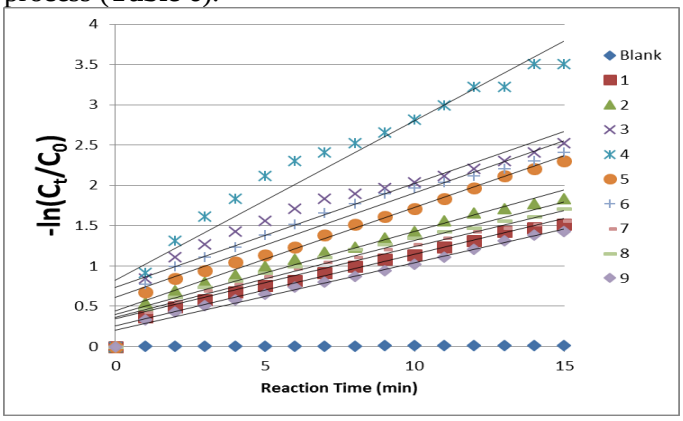

Fig. 7. Graph of $-\ln(C_t/C_0)$ versus reaction time of photodegradation of CR solution for the as-synthesized ZTZ nanocomposites

Table 6. Kinetic parameters of photodegradation of CR solution by the as-synthesized 1-9 ZTZ nanocomposites

Photocatalyst (ZTZ)	1	2	3	4	5	6	7	8	9
Rate constant (min^{-1})	0.089	0.103	0.129	0.197	0.128	0.129	0.089	0.095	0.084
Standard deviation	0.97	0.95	0.90	0.92	0.96	0.91	0.94	0.94	0.98
Half- time (min)	7.79	6.73	5.37	3.52	5.41	5.37	7.79	7.29	8.25
Adsorption capacity (mg/g)	15.6	16.8	18.4	19.4	18.0	18.2	15.8	16.4	15.2

3.12. Mechanism of photodegradation

Some factors affect the photodegradation properties of nanoparticles: (a) recombination of h^+/e^-on the surface, (b) aggregation of photocatalyst particles, and (c) size quantization effect. By decreasing the particle size, the density of recombination centers increases and leads to the recombination of holes and electrons. Furthermore, fine nanoparticles can be easily aggregated, and they can be directed to a decrease in the availability of active surface sites. The size quantization effect states that Eg increases as the particle size decreases, reducing photoactivity [37-39]. However, the surplus of defects can be affected inversely on the charge recombination rate. In addition, the amount of the band gap energy, CB and VB energy level is important in the semiconductor efficiency. When a photon of energy higher or equal to the band gap energy of the semiconductor is absorbed, an electron is promoted from the valence band to the conduction band with the simultaneous generation of a hole [40].

The hole/electron pair is very excited and they are recombinated very fast. One of the methods for increasing of recombination time is composition of semiconductors. In these ternary photocatalysts, the conduction band (CB) and valence band (VB) energy levels of TiO_2 and ZnO lay within the bandgap of ZrO_2; the h^+/e^-separation may take place in ZrO_2/TiO_2/ZnO ternary oxide. When the electrons are excited, most of the electrons from CB of ZrO_2 automatically transfer to the CB of ZnO and TiO_2; the h^+/e^- pair recombination may be delayed (**Fig. 8**). Thus, many holes can be trapped in the VB of ZnO and the VB of TiO_2 to induce oxidation of the dye molecules by forming various reactive oxygen species. In contrast, the electron centers are created in the CB of ZnO and TiO_2 as the reductive agents [34]. The holes on ZnO and TiO_2 (h^+VB) convert the water molecules to hydroxyl radicals, and the electrons on ZnO (e^-CB) and TiO_2 (e^-CB) produce the free radicals of O_2^{0-} and then H_2O_2 molecules are produced. Thereby, OH• radical, superoxide radical anion (O_2 •−), H_2O_2 molecule, and its conjugated acid (HO_2 •) will be produced. These radicals can react with pollutant molecules and disintegrate them into CO_2 and H_2O. Finally, the dye molecules are oxidized and mineralized [41]. The reactions mechanism can be described as below reaction:

$$ZrO_2/TiO_2/ZnO + h\nu \rightarrow ZrO_2/TiO_2/ZnO(e^-CB + h^+VB)$$

$$ZrO_2\,(h^+VB) + H_2O \rightarrow H^+ + OH^0$$

$$OH^0 + CR$$
→ Oxidation and mineralization of CR molecule

$$OH^0 + OH^0 \rightarrow H_2O_2$$

$$H_2O_2 + CR$$
→ Oxidation and mineralization of CR molecule

$$ZnO/TiO_2(e^-CB) + O_2 \rightarrow ZnO/TiO_2 + O_2^{0-}$$

$$O_2^{0-} + CR$$
→ Oxidation and mineralization of CR molecule

$$H^+ + O_2^{0-} \rightarrow HO_2^0$$

$$HO_2^0 + CR$$
→ Oxidation and mineralization of CR molecule

$$ZnO/TiO_2(e^-CB) + HO_2^0 \rightarrow HO_2^-$$

$$H^+ + HO_2^- \rightarrow H_2O_2$$

$$H_2O_2 + CR$$
→ Oxidation and mineralization of CR molecule

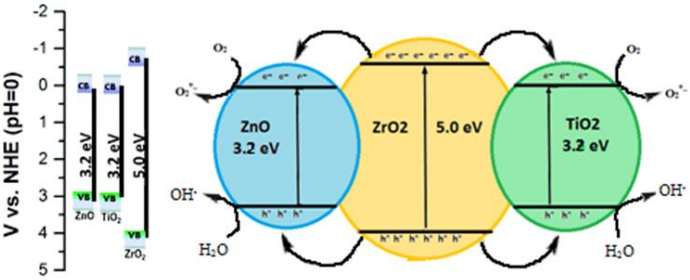

Fig. 8. Scheme of the photocatalytic mechanism of electron-hole pair separation of the as-synthesized ZTZ nanocomposites for photodegradation of CR

4. Conclusions

The Taguchi experimental design approach was utilized to find the optimal synthesis conditions of

$ZrO_2/TiO_2/ZnO$ ternary nanocomposites to remove CR from aqueous solution. An $L_9(3^4)$ OA was used to investigate the effect of four factors and their three levels, (1) the calcination temperature, (2) the aging time, (3) calcination time, and (4) the duration of ultrasonic irradiation, on photodegradation efficiency of CR solution. The effects of parameters were analyzed based on the photocatalytic efficiency. Then the optimal choice for each parameter was predicted by the Taguchi method. The results showed that increasing the specific surface area and reducing the particle size of nanocomposites were caused the enhancing of the PD%.

Acknowledgements

The authors express their thanks to East Tehran Branch, Islamic Azad University.

Conflict of Interest

The authors declare that they have no conflict of interest.

References

[1] W. Li, B. Mu, Y. Yang, Bioresource Technol., 277 (2019) 157–170.
[2] A. Nezamzadeh-Ejhieh, E. Shahriari, J. Ind. Eng. Chem., 20 (2014) 2719–2726.
[3] C.N.C. Hitam, A.A. Jalil, J. Environ. Manage, 258 (2020) 110050–110068.
[4] P.M. Dellamatrice, M.E. Silva-Stenico, L.A.B. de Moraes, M.F. Fiore, R.T.R. Monteiro, Braz. J. Microbiol., 48 (2017) 25-31.
[5] S. Zereshki, P. Daraei, A. Shokri, J. Hazard. Mater. 356 (2018) 1-8.
[6] A. Muleja, B. Mamba, J. Env. Chem. Eng., 6 (2018) 4850-4863.
[7] P. Nidheesh, M. Zhou, M.A. Oturan, Chemosphere, 197 (2018) 210-227.
[8] Y. Wang, Y. Pan, T. Zhu, A. Wang, Y. Lu, L. Lv, K. Zhang, Z. Li, Sci. Total. Environ. 634 (2018) 616-627.
[9] S.P. Ghuge, A.K. Saroha, J. Water Process Eng., 23 (2018) 217-229.
[10] M. Ahmad, E. Ahmed, Z. Hong, W. Ahmed, A. Elhissi, N. Khalid, Ultrason. Sonochem. 21 (2014) 761-773.
[11] D. Ayodhya, G. Veerabhadram, Mater. Today Energy, 9 (2018) 83-113.
[12] A. Nezamzadeh-Ejhieh, H. Zabihi-Mobarakeh, J. Ind. Eng. Chem., 20 (2014) 1421-1431.
[13] A. Buthiyappan, A. R. Abdul Aziz, W. M. Ashri Wan Daud, Rev Chem Eng 32 (2016) 1–47
[14] A. Nezamzadeh-Ejhieh, Z. Salimi, Appl. Catal. A-Gen., 390 (2010) 110–118.
[15] N. Arabpour, A. Nezamzadeh-Ejhieh, Mater. Sci. Semicond. Proces. 31 (2015) 684–692.
[16] S. Senobari, A. Nezamzadeh-Ejhieh, J. Mol. Liq., 257 (2018) 173-183.
[17] J. Tian, L. Chen, Y. Yin, X. Wang, J. Dai, Z. Zhu, X. Liu, P. Wu, Surf. Coat. Tech., 204 (2009) 205-214.
[18] B. Neppolian, Q. Wang, H. Yamashita, H. Choi Appl. Catal. A-Gen., 333 (2007) 264-271.
[19] C. S. Chou, C. Y. Ho, C. I. Huang, Adv. Powder Technol., 20 (2009) 55-61.
[20] C.-S. Chou, R.-Y. Yang, J.-H. Chen, S.-W. Chou, Powder Technol., 199 (2010) 264-271.
[21] M. Barmala, A. Moheb, R. Emadi, J Alloy Compd., 485 (2009) 778-782.
[22] Y. Q. Song, D. H. He, B. Q. Xu, Appl. Catal. A-Gen., 337 (2008) 19-28.
[23] X. Xu, J. Wang, J. Tian, X. Wang, J. Dai, X. Liu, Ceram. Int. 37 (2011) 2201-2206.
[24] S. Aghabeygi, M. Khademi-Shamami, Ultrason. Sonochem. 41 (2018) 458-465.
[25] A. Nezamzadeh-Ejhieh, M. Bahrami, Desalin. Water Treat. 55 (2015) 1096-1104.
[26] A.E. Kandjani, M.F. Tabriz, B. Pourabbas, Mater. Res. Bull., 43 (2008) 645-654.
[27] N. Arefian, A. Shokuhfar, M.R. Vaezi, A. Esmaielzadeh Kandjani, M. Farzalipour Tabriz, Defect Diffus. Forum, 273 (2008) 34-39.
[28] R. Mahdavi, S.S.A. Talesh, Ultrason. Sonochem. 39 (2017) 504-510.
[29] G.O. Oladipo, A.K. Akinlabi, S.O. Alayande, T.A. Msagati, H.H. Nyoni, O.O. Ogunyinka, Can. J. Chem., 97 (2019) 642-650.
[30] B. Manikandan, R. John, Iran. J. Catal. 10 (1), 2020, 1-16
[31] G. Zhou, J. Deng, Mat. Sic. Semicon. Proc., 10 (2007) 90-96.
[32] D. Ramírez-Ortega, A.M. Meléndez, P. Acevedo-Peña, I. González, R. Arroyo, Electrochim. Acta, 140 (2014) 541-549.
[33] C. Chen, P. Liu, C. Lu, Chem. Eng. J., 144 (2008) 509-513.
[34] N. Xiao, Z. Li, J. Liu, Y. Gao, Thin Solid Films, 519 (2010) 541-548.
[35] N. Ibrahim, S. Al-Shomar, S.H. Ahmad, Appl. Surf. Sci., 283 (2013) 599-602.
[36] B. Divband, A. Jodaie, M. Khatmian, Iran. J. Catal., 9 (1), 2019, 63-70.
[37] X. Zou, X. Li, Z. Qu, Q. Zhao, Y. Shi, Y. Chen, M. Tade, S. Liu, Mater. Res. Bull., 47 (2012) 279-284.
[38] S.M. Saleh, Spectrochim. Acta A, 211 (2019) 141-147.
[39] S. Klubnuan, S. Suwanboon, P. Amornpitoksuk, Opt. Mater., 53 (2016) 134-141.
[40] N. Omrani, A. Nezamzadeh-Ejhieh, M. Alizadeh, Desalin. Water Treat. 162 (2019) 290–302.
[41] B. M. Pirzada, N. A. Mir, N. Qutub, O. Mehraj, S. Sabir, M. Muneer, Mater. Sci. Eng: B, 193 (2015) 137-145.